Journal of ELECTRICAL ENGINEERING, VOL 66. NO 7/s, 2015, 193-198

USING THE SURROUNDING MAGNETIC FIELD IN DIAGNOSIS OF THE BLDC MOTOR

Przemysław Szulim* — Szymon Gontarz*

In this paper, the basis of a new method for the diagnosis of an electric motor was presented. First, a model of the BLDC motor was developed, and the most important steps to build it were presented. The model considers the electromagnetic behavior as well as mechanical faults. Theoretical calculation was verified by an FEM model. Finally, simulation results were presented.

Keywords: magnetic field, modeling, BLDC motor, diagnosis

1 INTRODUCTION

Diagnosis of Brushless DC (BLDC) motors is an interesting scientific task for which many methods have been adopted. The most intensively developed methods are still CSA (current signal analysis) methods [1], [2], vibrations analysis methods [3,4] and flux leakage methods [5]. To better understand the influence of faults on diagnostic symptoms, motor models are widely developed. Interesting analyses can be found in the literature [2], [6]–[9]. All faults related to BLDC motors can be distinguished as electric and mechanical faults. A drawback of many works is the high degree of approximation applied to the modelling of the motor and associated faults. An interesting approach to the modelling of BLDC motors has been developed over the last 40 years, mainly for motor design. In [10], [11], one can find a two-dimensional approach to analyze the magnetic field in the air-gap region of BLDC motors. Important works were presented in [12]–[15], in which the authors prepared the first comprehensive magnetic model of a motor considering field form Permanent Magnets (PM) and stator coils. Effects of the stator slots were also included via so-called relative permeance functions. Subsequent works dealt with the problem of considering stator slots. The results of these investigations can be found in works such as [12]–[15], in which the authors developed the so-called sub-domain model, wherein the domains referred to the air region created by the geometry of the stator slots. Significant contributions are also presented in [20], [21], where the influence of eccentricity on the field distribution was investigated. Future work considering this effect was also developed for the sub-domain model [22]–[24]. Nevertheless, the authors could not find complete models that include all important phenomena. Moreover, the effects of commutation and load pulsation were also not modelled. This has motivated the authors to build a complete model of work for BLDC motors that can allow the simulation of work conditions and the influence of the presence of current harmonics. In addition, the possibility of using an external magnetic field as a source of diagnostic information was the second aim of this work. The influence of mechanical faults such as eccentricity and demagnetization is also considered in this paper assuming constant and finite value of the permeability.

2 THEORY

The complete motor model can be described by three mutually bounded: mechanical, electric and magnetic submodels models. The mechanical model provides information regarding the rotor shaft position subject to internal magnetic torque and external load torque. In the analysis, all dynamics were neglected. The electric model considers the effect of the work of the electronic commutator as well as the electric part of the motor. In Fig. 1, one can see two separate regions of this sub-model. The shaded region represents a part of the electric commutator.

In each step, one pair of phases is energized and one stays floating.

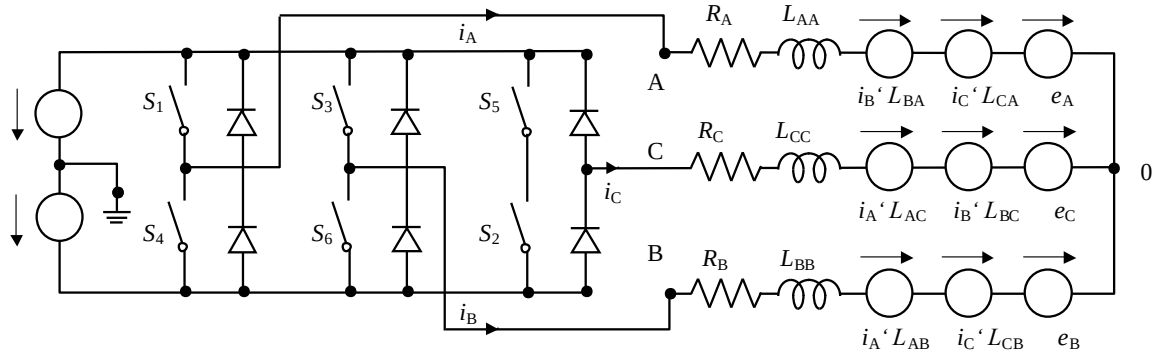

Fig. 1. Electric model of the motor

* Warsaw University of Technology, Faculty of Automotive, Institute of Vehicles, Poland, p.szulim@mechatronika.net.pl

ISSN 1335-3632

In this paper, the effects of current recirculation together with nonlinearities in switches were not considered. In the case of a three-phase motor, the complete sequence consists of six steps of commutation.

It is important to note that the electronic commutator can be embedded in the motor structure as well as exist as a stand-alone device. This feature is important for diagnosis because, in the case of an integrated system, one cannot directly measure phase currents without disassembly of the motor. The electric part of the motor (marked by the orange frame) was modelled by three linear equations

$$\begin{aligned} U_B &= R_B i_B + \frac{\mathrm{d}}{\mathrm{d}t}\left(L_{AB} i_A + L_{BB} i_B + L_{CB} i_C\right) + e_B \\ U_C &= R_C i_C + \frac{\mathrm{d}}{\mathrm{d}t}\left(L_{AC} i_A + L_{BC} i_B + L_{CC} i_C\right) + e_C \\ U_A &= R_A i_A + \frac{\mathrm{d}}{\mathrm{d}t}\left(L_{AA} i_A + L i_B + L_{CA} i_C\right) + e_A , \end{aligned} \tag{1}$$

where R are the resistance of the windings, i are the phase currents, L are the self and the mutual inductances, respectively and e are the electromotive forces. The magnetic motor model bears much more information then are the instantaneous values of the torque, electromagnetic force and inductance. To simplify the analysis, two-dimensional case is considered in this paper

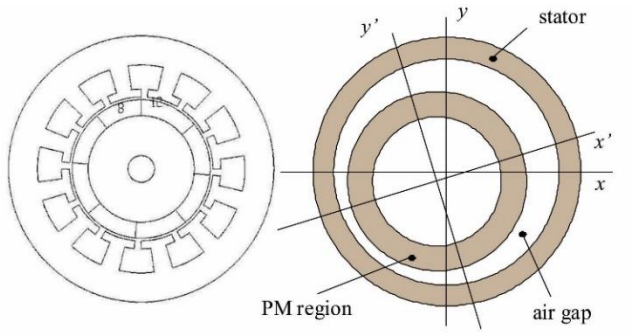

Fig. 2. Cross section of motor and geometry simplification

The cross-section of the motor is shown in Fig. 2. The slots in the stator were neglected and in six characteristic regions, one can put equations $\Delta\varphi = 0$ and $\mu_r \Delta\varphi = div\mathbf{M}$, using scalar magnetic potential φ, the magnetization vector $\mathbf{M}$, and μ_r - the relative permeability. First equation describes the potential in a region without sources (regions except the PM), and the second - permanent magnets. To find the solution of the PDE equations for each pair of six regions, boundary conditions must be specified:

$$\begin{aligned} \begin{bmatrix} \mu_i & 0 \\ 0 & 1 \end{bmatrix} \boldsymbol{H}^i\left(R_i,\theta\right) &= \begin{bmatrix} \mu_{i+1} & 0 \\ 0 & 1 \end{bmatrix} \boldsymbol{H}^{i+1}\left(R_i,\theta\right) \\ \begin{bmatrix} \mu_i & 0 \\ 0 & 1 \end{bmatrix} \boldsymbol{H}^i\left(R_i,\theta\right) &= \begin{bmatrix} \mu_3 & 0 \\ 0 & 1 \end{bmatrix} \boldsymbol{H}^{III}\left(R_2,\theta\right) + \mu_0 M\left(\theta\right) \\ \left(R_4,\theta\right)\begin{bmatrix} \mu_0 & 0 \\ 0 & 1 \end{bmatrix} + \begin{bmatrix} 0 \\ J \end{bmatrix} &= \boldsymbol{H}^V\left(R_4,\theta\right)\begin{bmatrix} \mu_5 & 0 \\ 0 & 1 \end{bmatrix} \end{aligned} \tag{2}$$

Where $\boldsymbol{H}^i\left(r,\theta\right) = \begin{bmatrix} H^r\left(r,\theta\right) \\ H^\theta\left(r,\theta\right) \end{bmatrix} = \begin{bmatrix} -\dfrac{\partial\varphi}{\partial r} \\ -\dfrac{1}{r}\dfrac{\partial\varphi}{\partial\theta} \end{bmatrix}$

J is the phase current density, $\boldsymbol{H}$ is the magnetic field vector , and r,θ are the main coordinates of the stator system. Equation (2) represents a special case of the more general form

$$\begin{aligned} \mathbf{n}\times\mathbf{H}^{IV} &= \mathbf{n}\times\mathbf{H}^{III} \\ \mathbf{n}\cdot\mathbf{B}^{IV} &= \mathbf{n}\cdot\mathbf{B}^{III} \end{aligned} \tag{3}$$

where $\mathbf{n}$ is the normal boundary vector. Equations (3) describe the field between two regions without sources, the region with a source and the air gap-stator region in the given order. Based on a concept of thin current sheet, the field induced by the stator coils was modelled, [13]. Using the method of variables separation the solution for the scalar magnetic potential can be found in all discussed regions. This will lead to a task of determining unknown coefficients $A_n^I \ldots B_n^{VI}$ that can be calculated using the Fourier expansion, and a clear form of the two matrix equations will be obtained

$$\begin{aligned} \mathbf{A}\cdot\mathbf{X}_a &= \mathbf{I}M_n^C \\ \mathbf{A}\cdot\mathbf{X}_b &= \mathbf{I}M_n^S \end{aligned} \tag{4}$$

where M_n^C, M_n^S are the Fourier expansion coefficients describing the magnetization vector , $\mathbf{A}$ is a 10×10 matrix of geometrical and magnetic motor parameters, $\mathbf{X}_a$ and $\mathbf{X}_b$ are vectors of required coefficients

$$\begin{aligned} \mathbf{X}_a^T &= \left[A_n^I, A_n^{II}, B_n^{II}, A_n^{III}, B_n^{III}, A_n^{IV}, B_n^{IV}, A_n^V, B_n^V, A_n^{VI}\right] \\ \mathbf{X}_b^T &= \left[B_n^I, C_n^{II}, D_n^{II}, C_n^{III}, D_n^{III}, C_n^{IV}, D_n^{IV}, C_n^V, D_n^V, B_n^{VI}\right] \\ \mathbf{I}^T &= \left[0,0,\frac{\mu_0}{n(n^2-1)},\frac{1}{\mu_r(n^2-1)},\frac{\mu_0}{n(n^2-1)},\frac{1}{\mu_r(n^2-1)},0,0,0,0\right] \end{aligned} \tag{5}$$

From above equations, the magnetic field generated by the PM can be calculated in each region. In the magnet region, to describe the magnetization vector for each pole, Fourier expansion was used. In Fig. 3, one can see the influence of different numbers of coefficients on the shape of the curve. This curve represent the amplitude and sign of the magnetization vector due to θ angle (θ-r reference coordinate system).

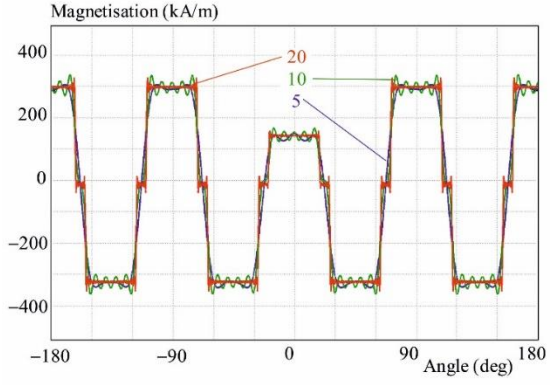

Fig. 3. Different number of the expansion sum terms to shape the magnetization curve

Moreover, at this stage, the effect of demagnetization was modelled. The complete equation of magnetization can be shown as follows

$$M(\theta) = M_0 + \sum_{n=1}^{\infty}\left(M_n^C cos(n\theta) + M_n^S si\right) \tag{6}$$

$$M_n^C = M^C(n)\cos(n\theta')$$

$$M_n^S = M^C(n) sin(n\theta')$$

$$= \frac{2}{n\pi} sin\left(\frac{n\pi}{2p(1+k)}\right)\begin{bmatrix} M_D + (-1)^n M_M + \\ 2M_M \sum_{i=2}^{p}(-1)^{i-1} cos\left(n(i-1)\frac{\pi}{p}\right)\end{bmatrix} \tag{7}$$

$$M_0 = \frac{1}{2p(1+k)}(M_D - M_M) \tag{8}$$

θ' is the rotor shift angle, p is the number of pole pairs, M_M is the magnetization of the magnets, M_D is the magnetization of the demagnetized magnet, and k is the pole-arc-to-pole-pitch ratio. Equation (6) describes the radial magnetization of PM. The important problem of eccentricity modeling was solved by a few steps of approximation. The idea presented in paper [20] was used. In Fig. 4, one can see two coordinate systems shifted and rotated mutually what corresponds to the shift of the motor rotor relative to the stator in 2-D model. The θ'-r' coordinate system is connected with the rotor. The parameters ε and α describe the relative shift with respect to the main stator coordinate system $\theta - r$.

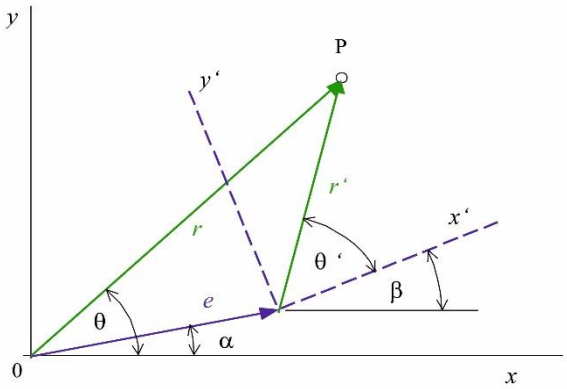

Fig. 4. Relation between two coordinate systems

These parameters determine the type of eccentricity, *ie*, static eccentricity (ε > 0 and const., α = const.) or dynamic eccentricity (ε > 0 and const., $\alpha = f(t)$). The approximate relation between these systems is described by the equations below.

$$\begin{aligned} r' &= r - \varepsilon\cos(\theta-\alpha) + O\left(\varepsilon^2\right) \\ \theta' &= \theta - \beta + \frac{\varepsilon}{r} sin(\theta-\alpha) + O\left(\varepsilon^2\right) \\ \theta &= \theta' + \beta - \frac{\varepsilon}{r'} sin(\theta'+\beta-\alpha) + O\left(\varepsilon^2\right) \\ r &= r' + \varepsilon\cos(\theta'+\beta-\alpha) + O\left(\varepsilon^2\right) \end{aligned} \tag{9}$$

Because the simplified boundary equations (4) are not valid in the case of eccentricity, the generalized form (2) must be used. For boundaries at the radii $r = R_1, R_2, R_3$, one must calculate the normal vector equation

$$\mathbf{n}(r,\theta) = \frac{\nabla f}{|\nabla f|} = \begin{bmatrix} \frac{1}{n_m}\mathbf{u}_r \\ \frac{\varepsilon}{r}\frac{sin(\theta-\alpha)}{n_m}\mathbf{u}_\theta \end{bmatrix} \tag{10}$$

$$f(r,\theta,\varepsilon,\alpha) = r - \varepsilon\cos(\theta-\alpha) - R_i = 0, \quad i = 1,2,3 \tag{11}$$

$$n_m = \sqrt{1 + \left(\frac{\varepsilon}{r} sin(\theta-\alpha)\right)^2}$$

Using (3) and (10), one can determine the general form for the boundary conditions

$$\begin{aligned} &H^{\theta[i+1]} - \frac{\varepsilon}{r}\sin(\theta-\alpha)H^{r[i+1]} = \\ &= H^{\theta[i]} - \frac{\varepsilon}{r}\sin(\theta-\alpha)H^{r[i]} \\ &B^{r[i+1]} - \sin(\theta-\alpha)B^{\theta[i+1]} = \\ &= B^{r[i]} - \sin(\theta-\alpha)B^{\theta[i]} \end{aligned}\Bigg|_{r=r'} \tag{12}$$

Equations (12) are still difficult to solve because of the complicated form of the r variable. It is important to note that only radius deformation due to eccentricity was included in the calculation and that phase deformation was neglected because of its weak impact on the magnetic field in the case of a relatively thin air gap region. The other two boundaries can by described by equations (2). To simplify equation (12), a perturbation method was used. This approach allows the potential and magnetic field equation to be expressed in the form of the sum of different-order solutions

$$\varphi^i(r,\theta) = \varphi^i_{(0)}(r,\theta) + \varepsilon\varphi^i_{(1)}(r,\theta) + \ldots$$

It is worth noting that only zero- and first-order expansion was considered. Using the perturbation method and the Taylor expansion of (12) around R_i, a new boundary condition can be determined

$$\begin{aligned} &\frac{\partial\varphi^i_{(1)}}{\partial\theta} - \frac{\partial\varphi^{i+1}_{(1)}}{\partial\theta} = sin(\theta-\alpha)\left(\frac{\partial\varphi^i_{(0)}}{\partial r} - \frac{\partial\varphi^{i+1}_{(0)}}{\partial r}\right) + \\ &\cos(\theta-\alpha)\left(\frac{\partial^2\varphi^{i+1}_{(0)}}{\partial r\partial\theta} - \frac{\partial^2\varphi^i_{(0)}}{\partial r\partial\theta} + \frac{\partial\varphi^i_{(0)}}{\partial\theta} - \frac{\partial\varphi^{i+1}_{(0)}}{\partial\theta}\right) \end{aligned} \tag{13}$$

$$\begin{aligned} &\mu_i\frac{\partial\varphi^i_{(1)}}{\partial r} - \mu_{i+1}\frac{\partial\varphi^{i+1}_{(1)}}{\partial r} = \\ &sin(\theta-\alpha)\frac{1}{r^2}\left(\mu_{i+1}\frac{\partial\varphi^{i+1}_{(0)}}{\partial\theta} - \mu_i\frac{\partial\varphi^i_{(0)}}{\partial\theta}\right) + \\ &\cos(\theta-\alpha)\left(\mu_{i+1}\frac{\partial^2\varphi^{i+1}_{(0)}}{\partial r^2} - \mu_i\frac{\partial^2\varphi^i_{(0)}}{\partial r^2}\right) \end{aligned} \tag{14}$$

Index (0) or (1) indicates the zero- and first-order solutions. It is important to note that the first-order perturbation solution is

presented as a function of the zero-order solution. The zero-order solution can be calculated from (13). The full perturbed solution can be calculated from the two equations below, where $\mathbf{X}_{a(1)}$ and $\mathbf{X}_{b(1)}$ represent vectors of the wanted coefficients.

$$\mathbf{A}\cdot\mathbf{X}_{a(1)} = \sin(\alpha-\theta)\left(\mathbf{E}\cdot\mathbf{X}_{b(0)} + \mathbf{J}M_n^S\right) + \cos(\alpha-\theta)\mathbf{F}\cdot\mathbf{X}_{a(0)} - \mathbf{I}M_n^C \tag{15}$$

$$\mathbf{A}\cdot 0_{b(1)} = -\sin(\alpha-\theta)\left(\mathbf{E}\cdot\mathbf{X}_{a(0)} + \mathbf{J}M_n^C\right) + \cos(\alpha-\theta)\mathbf{F}\cdot\mathbf{X}_{b(0)} - \mathbf{I}M_n^S \tag{16}$$

where **E**, **F** and **J** are adequate matrixes or vector created based on motor magnetic and geometric properties. It is worth noting that equations (15) and (16) represent the solution for the field induced by the PM magnets. For the field generated by the current coils, the required coefficients can be calculated from the following equations

$$\mathbf{A}\cdot\mathbf{X}_{a(0)} = \mathbf{I}^{\boldsymbol{S}} J_S^S$$
$$\mathbf{A}\cdot\mathbf{X}_{b(0)} = \mathbf{I}^{\boldsymbol{S}} J_C^S \tag{17}$$
$$\mathbf{A}\cdot\mathbf{X}_{a(1)} = \sin(\alpha-\theta)\mathbf{E}\cdot\mathbf{X}_{b(0)} + \cos(\alpha-\theta)\mathbf{F}\cdot\mathbf{X}_{a(0)}$$
$$\mathbf{A}\cdot\mathbf{X}_{b(1)} = -\sin(\alpha-\theta)\mathbf{E}\cdot\mathbf{X}_{a(0)} + \cos(\alpha-\theta)\mathbf{F}\cdot\mathbf{X}_{b(0)}$$

$$\boldsymbol{I}^{\boldsymbol{S}} = \left[0,0,0,0,0,0,\frac{1}{n},0,0\right]^T$$

$$J_S^S(n) = J_s(n)\left(i_a + i_b\cos\left(n\frac{2}{3}\pi\right) + i_c\cos\left(n\frac{4}{3}\pi\right)\right)$$

$$J_C^S(n) = J_s(n)\left(i_b\sin\left(n\frac{2}{3}\pi\right) + i_c\sin\left(n\frac{4}{3}\pi\right)\right)$$

$$J_s(n) = \frac{-4}{R_4\alpha_S\pi n}sin\left(n(\alpha_S+\alpha_Z)\right)sin(n\alpha_S)$$

i_a, i_b i_c are the phase A, B, C currents. In Fig. 5, a comparison of the calculated model and the FEM model air gap radial field is presented. In this case, the effect of the stator sots was neglected, and only the field induced by the PM was considered. Both plots fit together. In Fig. 6, one can see a comparison of the radial-air gap region magnetic field generated by the PM. The effect of eccentricity was considered. Once again, both curves fit together. In Fig. 7, one can see the magnetic field in the air gap region generated by the phase current. In this case, the effect of the stator slot was included in the analytical model by the so-called relative permeance function [14]. This time, one can observe that both curves fit quite well. Differences exist and are the result of the imprecise approximation of the slots effect. Now it was possible to predict outer magnetic field in outer region. To simplify analysis only resultant equations will be presented. External magnetic field has two sources. One comes from permanent magnets and second from stator coils.

Equations (18) describe magnetic field produced by magnets

$$H_\theta^R(r,0)^{VI} = \sum_{n=1}^{\infty} nr^{-n-1}M^C(n)\begin{bmatrix} a_1\varepsilon sin(\omega_\alpha t)cos\left(n(\omega_{\theta'}t)\right) \\ +a_2\varepsilon cos(\omega_\alpha t)sin\left(n(\omega_{\theta'}t)\right)+ \\ a_3(1+\varepsilon)sin\left(n(\omega_{\theta'}t)\right)\end{bmatrix}, \tag{18}$$

where: a_1, a_2, a_3 are coefficient after the simplification, $\omega_{\theta'} = \theta'$, $\omega_\alpha = \dot{\alpha}$. First important property of such description is presented effect which is similar to amplitude modulation (AM) where $\omega_{\theta'}$ could be a carrier pulsation and which appears due to dynamic eccentricity can be treated as a modulating pulsation. Anyway this equation represents pure modulation equation only for some special cases for particular value of a_1 and a_2 (parameters close related to motor geometry and magnetic properties). In general frequency spectrum of such signal is similar to spectrum of AM signal but in this case modulation harmonics could have different amplitudes. This effect can be observed on the spectrum of magnetic signal both from simulation as well from experiment.

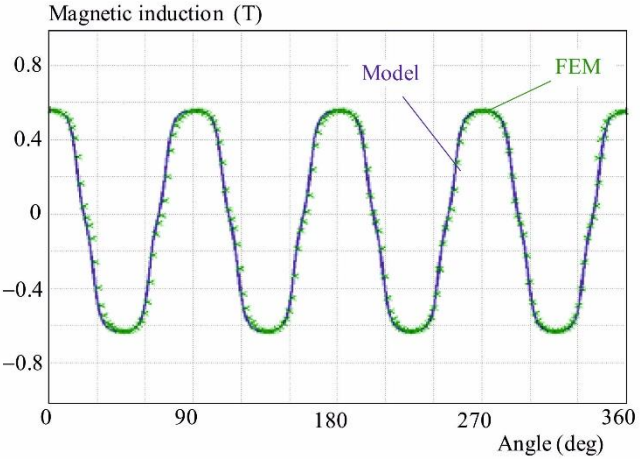

Fig. 5. Radial component of the magnetic induction in the air gap

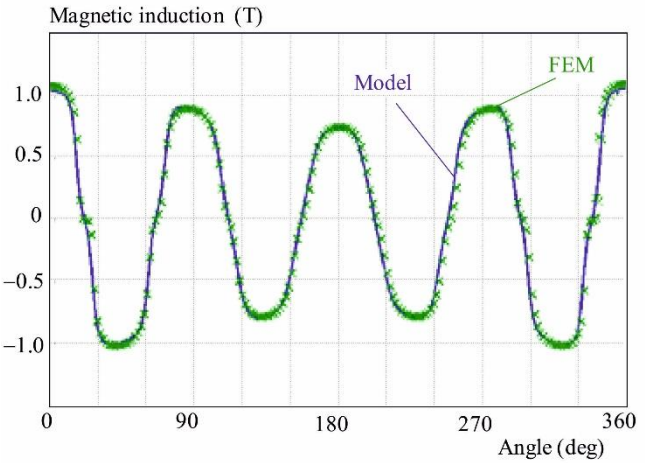

Fig. 6. Influence of eccentricity on radial magnetic field in the air gap

Another important property of signal described by equations (18) is that both together can be treated as an analytical Hilbert signal. This feature can be used to easy AM demodulation what could be described as follows

$$H_{\theta}^{RVI2} + H_{r}^{RVI2} \cong$$
$$r^{-2} M^{C}(n)^{2} \begin{bmatrix} cos^{2}(\omega_{\alpha} t)\left(a_{2}^{2} - a_{1}^{2}\right) \\ +2a_{1}a_{3}cos(\omega_{\alpha} t) + a_{1}^{2} + a_{3}^{2} \end{bmatrix} \quad (19)$$

Equation (19) is simplification of sum of squares of radial end tangential field component for only one "n" coefficient.

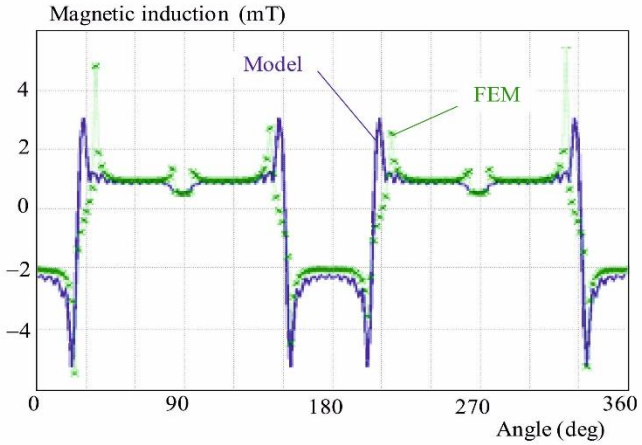

Fig. 7. Magnetic induction generated by the stator coils in the air gap region

Signal in form (19) relates only on dynamic eccentricity pulsation and is independent on rotor rotation speed, what is a great advantage. Of course the sum presented in (19) could be valid only in case of single carrier harmonic. Anyway amplitude of 4th harmonic is much greater than others and this difference grows when the distance from the motor is larger.

$$\boldsymbol{H}^{S}(r,0)^{VI} =$$
$$= \begin{bmatrix} -\sum_{n=1}^{\infty} n r^{-n-1} i_{ab} J_{s}(n) \begin{bmatrix} b_{1}(n) + \varepsilon sin(\omega_{\alpha} t) b_{2}(n) \\ +\varepsilon cos(\omega_{\alpha} t) b_{3}(n) \end{bmatrix} \\ \sum_{n=1}^{\infty} n r^{-n-1} i_{ab} J_{s}(n) \begin{bmatrix} c_{1}(n) - \varepsilon sin(\omega_{\alpha} t) c_{2}(n) \\ +\varepsilon cos(\omega_{\alpha} t) c_{3}(n) \end{bmatrix} \end{bmatrix} \quad (20)$$

Equation (20) describe two components of second source of outer magnetic field (current flows by *a* and *b* phase coils). Because of the high complexity of inductance end electromotive force, analytical description of phase currents weren't calculated. Important feature of signal (20) is fact that it can be treated as an AM modulation where carrier signal is a current and modulation signal comes from dynamic eccentricity. It is important to note that radial end tangential component of magnetic field have different amplitudes of carrier and modulation harmonics. So the total outer magnetic field appears as a sum of two fields described by (19) and (20). Static eccentricity leads to appear a change of magnetic field signal in space (relative to θ) but not in time. This is the reason why such effect cannot be easy distinguished by magnetic field observation. Demagnetization effect is revealed as a additional main harmonic in the field of spectrum and it doesn't leads to modulation effects.

3 SIMULATION

The complete model was built in the MATLAB environment. As mentioned earlier, only the simple linear part of the electric model was considered. The rotary speed was set to a constant or pulsating value depending on the test. In Fig. 8, the effect of the influence of eccentricity on the outer magnetic field is shown. One can observe a characteristic modulation effect. More precisely, this is an amplitude modulation. Corresponding effect can be also observed in current signal. Initially such phenomenon (observed in experiment) supposed to be the product of the simultaneous presence of both AM and PM modulation.

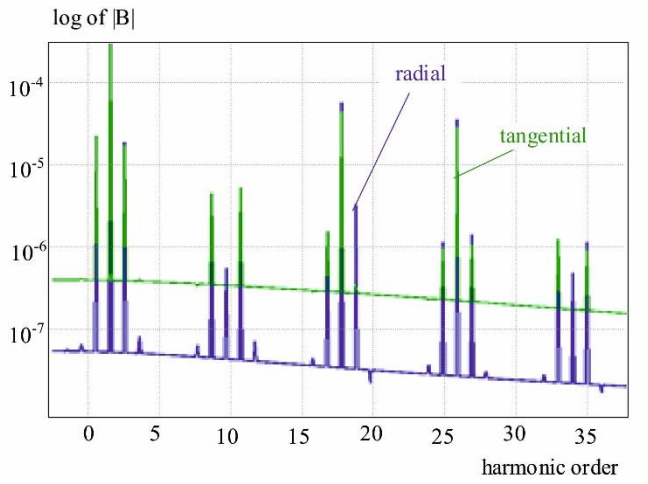

Fig. 8. Frequency spectrum of the outer magnetic field

Finally, model analysis proves that it is close related to AM only. A similar effect can be observed by the influence of demagnetization. In case of simulation of both faults, additional rotation harmonic appears together with modulation harmonics around them.

4 EXPERIMENTS

In an experiment, a BLDC motor (Dunkermotoren BG75x75) was investigated on a test stand. During the experiment, three degrees of eccentricity were applied (0.0 mm, 0.25 mm and 0.5 mm). The current, vibrations, noise and external magnetic field were measured for many types of work conditions. To conduct magnetic measurements, a three-axis fluxgate sensor was used. In Fig. 9, one can see the frequency spectrum of the magnetic signal (the radial

component). One can see again that dominate 4,12,20 and 28 harmonic and modulation harmonic around.
This observation agreed with the model and (6), where only an odd coefficient multiplied by the pole pair number exists.

5 CONCLUSION

In this paper, a model-based approach for the task of BLDC motor diagnosis was presented. First, the general model, sub-models and mutual connections were depicted. The most difficult part, *ie*, the magnetic model, was presented more precisely.

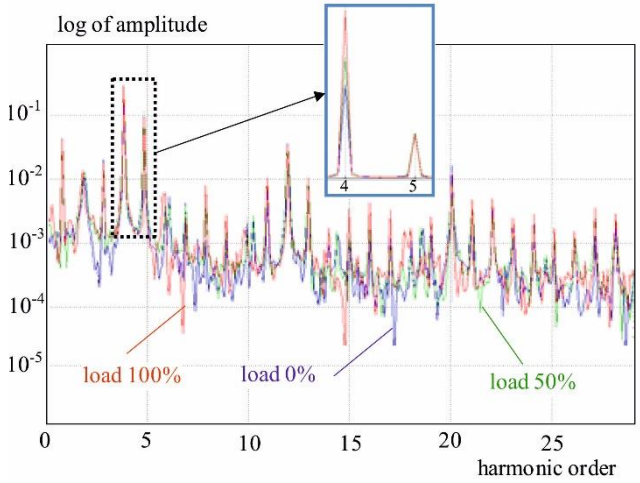

Fig. 9. Frequency spectrum of magnetic field signal experiment

Simulation results and experimental results were compared, and the basic observations were expanded on. It was possible for registered signals to carry diagnostic information, not only in terms of changes in a quasi-static field but also the dynamic changes of the field surrounding the electric motor operating at full speed.

The application supported by the analytical model is the enablement of observation and analysis of the changes of the magnetic field's parameters in space while accounting for the information regarding a momentary position of the electrical motor shaft, which substantially enhances

[1] A. Tashakori and M. Ektesabi, 'Fault diagnosis of in-wheel BLDC motor drive for electric vehicle application', *Intell. Veh. Symp. IV 2013 IEEE*, pp. 925–930, Jun. 2013.

[2] M. Blödt, P. Granjon, B. Raison, and J. Regnier, 'Mechanical fault detection in induction motor drives through stator current monitoring-theory and application examples', *Fault Detect.*, pp. 451–488, 2010.

[3] Jun-Kyu Park, Kyung-Tae Kim, Byeong-Woo Kim, and Jin Hur, 'Characteristic analysis of Inter-turn Fault in IPM and SPM-type BLDC motor', *Veh. Power Propuls. Conf. VPPC 2012 IEEE*, pp. 176–180, Oct. 2012.

[4] J. Dybała and A. Gałęzia, 'A Novel Method of Gearbox Health Vibration Monitoring Using Empirical Mode Decomposition', in *Advances in Condition Monitoring of Machinery in Non-Stationary Operations*, G. Dalpiaz, R. Rubini, G. D'Elia, M. Cocconcelli, F. Chaari, R. Zimroz, W. Bartelmus, and M. Haddar, Eds. Springer Berlin Heidelberg, 2014, pp. 225–234.

[5] D. Belkhayat, R. Romary, M. El Adnani, R. Corton, and J. F. Brudny, 'Fault diagnosis in induction motors using radial magnetic field measurement with an antenna', *Meas. Sci. Technol.*, vol. 14, no. 9, p. 1695, 2003.

[6] M. BLODT, *Condition Monitoring of Mechanical Faults in Variable Speed Induction Motor*. DEA Genie Electrique de l'Institut National Polytechnique de Grenoble.

[7] S. Nandi and H. A. Toliyat, 'Condition monitoring and fault diagnosis of electrical machines-a review', in *Industry Applications Conference, 1999. Thirty-Fourth IAS Annual Meeting. Conference Record of the 1999 IEEE*, 1999, vol. 1, pp. 197–204.

[8] H. E. Toliyat and S. Nandi, *Electric Machines, Modeling, Condition monitoring and Fault Diagnosis*. CRC Press, 2005.

[9] Kyung-Tae Kim, Jin Hur, and Gyu-Hong Kang, 'Inter-turn fault analysis of IPM type BLDC motor using fault impedance modeling', *Power Electron. ECCE Asia ICPE ECCE 2011 IEEE 8th Int. Conf. On*, pp. 2216–2224, May 2011.

[10] N. Boules, 'Two-dimensional field analysis of cylindrical machines with permanent magnet excitation', *Ind. Appl. IEEE Trans. On*, no. 5, pp. 1267–1277, 1984.

[11] N. Boules, 'Prediction of no-load flux density distribution in permanent magnet machines', *Ind. Appl. IEEE Trans. On*, no. 3, pp. 633–643, 1985.

[12] Z. Q. Zhu, D. Howe, E. Bolte, and B. Ackermann, 'Instantaneous magnetic field distribution in brushless permanent magnet DC motors. I. Open-circuit field', *Magn. IEEE Trans. On*, vol. 29, no. 1, pp. 124–135, 1993.

[13] Z. Q. Zhu and D. Howe, 'Instantaneous magnetic field distribution in brushless permanent magnet DC motors. II. Armature-reaction field', *Magn. IEEE Trans. On*, vol. 29, no. 1, pp. 136–142, 1993.

[14] Z. Q. Zhu and D. Howe, 'Instantaneous magnetic field distribution in brushless permanent magnet DC motors. III. Effect of stator slotting', *Magn. IEEE Trans. On*, vol. 29, no. 1, pp. 143–151, 1993.

[15] Z. Q. Zhu and D. Howe, 'Instantaneous magnetic field distribution in permanent magnet brushless DC motors. IV. Magnetic field on load', *Magn. IEEE Trans. On*, vol. 29, no. 1, pp. 152–158, 1993.

[16] Z. Q. Zhu, D. Howe, and C. C. Chan, 'Improved analytical model for predicting the magnetic field distribution in brushless permanent-magnet machines', *Magn. IEEE Trans. On*, vol. 38, no. 1, pp. 229–238, 2002.

[17] Z. J. Liu and J. T. Li, 'Analytical Solution of Air-Gap Field in Permanent-Magnet Motors Taking Into Account the Effect of Pole Transition Over Slots', *IEEE Trans. Magn.*, vol. 43, no. 10, pp. 3872–3883, Oct. 2007.

[18] T. Lubin, S. Mezani, and A. Rezzoug, 'Exact Analytical Method for Magnetic Field Computation in the Air Gap of Cylindrical Electrical Machines Considering Slotting Effects', *IEEE Trans. Magn.*, vol. 46, no. 4, pp. 1092–1099, 2010.

[19] Z. Q. Zhu, L. J. Wu, and Z. P. Xia, 'An Accurate Subdomain Model for Magnetic Field Computation in Slotted Surface-Mounted Permanent-Magnet Machines', *Magn. IEEE Trans. On*, vol. 46, no. 4, pp. 1100–1115, Apr. 2010.

[20] U. Kim and D. K. Lieu, 'Magnetic field calculation in permanent magnet motors with rotor eccentricity: without slotting effect', *Magn. IEEE Trans. On*, vol. 34, no. 4, pp. 2243–2252, 1998.

[21] U. Kim and D. K. Lieu, 'Magnetic field calculation in permanent magnet motors with rotor eccentricity: with slotting effect considered', *Magn. IEEE Trans. On*, vol. 34, no. 4, pp. 2253–2266, 1998.

[22] J. T. Li, Z. J. Liu, and L. H. A. Nay, 'Effect of Radial Magnetic Forces in Permanent Magnet Motors With Rotor Eccentricity', *IEEE Trans. Magn.*, vol. 43, no. 6, pp. 2525–2527, Jun. 2007.

[23] J. Fu and C. Zhu, 'Subdomain Model for Predicting Magnetic Field in Slotted Surface Mounted Permanent-Magnet Machines With Rotor Eccentricity', *IEEE Trans. Magn.*, vol. 48, no. 5, pp. 1906–1917, May 2012.

[24] S. Radkowski and M. Jasinski, 'Use of Condition Monitoring in the Proactive Maintenance Strategy', in *Engineering Asset Management - Systems, Professional Practices and Certification*, P. W. Tse, J. Mathew, K. Wong, R. Lam, and C. N. Ko, Eds. Springer International Publishing, 2015, pp. 601–610.

Received 30 November 2015